Int. J. Heat Mass Transfer. Vol. 30, No. 12, pp. 2571–2581, 1987
Printed in Great Britain

0017–9310/87 $3.00 + 0.00

Natural convective heat transfer in a rectangular porous cavity with variable fluid properties—validity of the Boussinesq approximation

M. B. PEIROTTI, M. D. GIAVEDONI and J. A. DEIBER
Instituto de Desarrollo Tecnológico para la Industria Química,
Güemes 3450, 3000 Santa Fe, Argentina

(*Received* 15 *December* 1986 *and in final form* 27 *April* 1987)

Abstract—In this work, the applicability of the Boussinesq approximation is investigated for natural convection in a fluid-saturated porous cavity with vertical walls maintained at two different temperatures and horizontal walls completely insulated. Numerical calculations are performed for two different fluids of practical interest, water and air, in a wide range of Rayleigh numbers and aspect ratios. Flow and temperature fields and heat transfer rates obtained through the evaluation of a model that includes fluid temperature dependent properties, are presented. One of the most important conclusions is that the Nusselt number evaluated through the Boussinesq approximation can be substantially different from the Nusselt number obtained with this model.

INTRODUCTION

NATURAL convection in porous media is a fundamental problem associated with various practical applications; in particular, it has received special attention in geothermal reservoir exploitation, high performance insulation building, and heat exchangers. Within this context of research a thoroughly numerical study concerning the convective heat transfer in rectangular porous cavities of low aspect ratio ($A < 1$), with vertical walls maintained at two different temperatures and horizontal walls completely insulated, has been recently published in the literature [1]. In this mentioned work, Darcy's law is assumed to hold and the porous cavity is filled with a normal Boussinesq fluid. Other numerical and analytical results have also been reported for square and tall porous cavities ($A \geqslant 1$) under the same physical assumptions as those used in the work of Prasad and Kulacki [1] (see, also, refs. [2–4]).

Since the validity of assumptions in the formulation and solution of physical problems can be verified by the use of high-speed modern computers, there exist now research motivations to study the limits of applicability of the Boussinesq approximation associated with the Newtonian fluid flow in a porous cavity. Within this scope, Gartling and Hickox [5] used a numerical method to examine the changes in flow and temperature fields and heat transfer rates of a water saturated square porous bed ($A = 1$) for the following mathematical models: (1) the Boussinesq approximation is retained, (2) this approximation is relaxed to account for the variability of fluid viscosity and thermal conductivity (extended system), and (3) the Boussinesq approximation is not used (complete system).

Nevertheless, it has to be pointed out here that the complete system analyzed by Gartling and Hickox [5] does not include the effects of pressure variations owing to changes in fluid density; this term can be important under certain physical situations as it will be shown in this work. Also, the results reported by these authors only cover a range of Rayleigh numbers between 0 and 300, and appreciable numerical differences between Nusselt numbers of the above mentioned models are not observed.

We present here a numerical study concerning the natural convective heat transfer in a rectangular porous cavity ($0.3 \leqslant A \leqslant 3$). The Boussinesq approximation is eliminated because under certain conditions the product between the isobaric coefficient of fluid thermal expansion β and the difference between the hot and cold wall temperatures ΔT is not necessarily negligible. Moreover, all the fluid properties are allowed to change with temperature. Although the principal difference of this model with that proposed by Gartling and Hickox [5] consists of the inclusion of the pressure work in the thermal energy equation, we have been able to compute our model at very large Rayleigh numbers ($0 < Ra^* \leqslant 10\,000$, which is the same range of values analyzed in ref. [1]) for two different fluids of practical interest, water and air. Thus, our calculations include a fluid with a viscosity that decreases with temperature and a fluid with the opposite trend. Therefore, important physical conclusions can be obtained concerning the effects of viscosity change with temperature on Nusselt numbers and flow fields, as it will be shown in this work.

Results are also presented for typical Rayleigh numbers found in geothermal reservoirs. Comparison of flow and temperature fields and heat transfer rates obtained through numerical evaluations are carried

NOMENCLATURE

A	aspect ratio, L/D
B	dimensionless isobaric coefficient of thermal expansion, $\beta\Delta T$
c	specific heat of fluid at constant pressure [J kg^{-1} °C^{-1}]
D	width of porous cavity [m]
F	dimensionless effective conductivity
g	acceleration due to gravity [m s^{-2}]
$\bar{h}$	average heat transfer coefficient on heated wall, $q/(T_h - T_c)$ [W m^{-2} °C^{-1}]
K	permeability of porous medium [m^2]
k_m	effective thermal conductivity of the saturated porous medium [W m^{-1} °C^{-1}]
k	fluid conductivity [W m^{-1} °C^{-1}]
k_s	solid conductivity [W m^{-1} °C^{-1}]
L	height of porous cavity [m]
M	dimensionless viscosity
M_w	molecular weight [kg kmol^{-1}]
Nu	Nusselt number based on cavity width, hD/k_m
p	pressure [Pa]
q	heat transfer rate per unit area [W m^{-2}]
R	dimensionless density
Ra^*	Rayleigh number based on cavity width, $\rho g\beta KD\Delta T/(\mu\alpha)$
R_g	gas-law constant [J kg^{-1} °C^{-1}]
T	temperature [°C]
ΔT	temperature difference, $T_h - T_c$ [°C]
U	characteristic velocity, $k_{mh}/(\rho_h cD)$ [m s^{-1}]
u	fluid velocity in x-direction, $(-\alpha/RD)(\partial\psi/\partial Y)$ [m s^{-1}]
v	fluid velocity in y-direction, $(\alpha L/RD^2)(\partial\psi/\partial X)$ [m s^{-1}]
$\mathbf{v}$	superficial velocity vector [m s^{-1}]
x, y	Cartesian coordinates [m]
X	dimensionless distance on x-axis, x/D
Y	dimensionless distance on y-axis, y/L.

Greek symbols

α	thermal diffusivity of porous medium, $k_m/\rho c$ [m^2 s^{-1}]
β	isobaric coefficient of thermal expansion of fluid [°C^{-1}]
γ	$(1/\rho_h c)(\partial p/\partial T)_\rho$
ξ, η	dimensionless stretched coordinates
Λ	$T_c/(T_h - T_c)$
μ	dynamic viscosity of fluid [kg m^{-1} s^{-1}]
θ	dimensionless temperature, $(T - T_c)/(T_h - T_c)$
ρ	density of fluid [kg m^{-3}]
ϕ	porous medium porosity
ψ	stream function.

Subscripts

c	cooled wall
h	heated wall
i, j	spatial position in the computational mesh
n	number of iteration.

out by computing the model with and without the Boussinesq approximation. These comparisons show differences in the heat transfer rate, evaluated through the Nusselt number, which are greater than 30%. It is also important to mention here that different flow structures were found due to the dependence of fluid viscosity with temperature.

MODEL FORMULATION AND SOLUTION

The system, which is the same as that of Prasad and Kulacki [1], consists of a fluid saturated porous medium enclosed by two vertical isothermal walls at T_h and T_c with $T_h > T_c$, and two adiabatic horizontal walls. Heat is transferred in and out of the porous cavity in steady state. Since the Boussinesq approximation is eliminated, conservation of mass implies

$$\nabla \cdot (\rho \mathbf{v}) = 0 \tag{1}$$

where the fluid density ρ is a non-linear function of temperature T. It is also assumed that the Newtonian fluid moves slowly, so that Darcy's law applies

$$\mathbf{v} = \frac{k}{\mu}(-\nabla p + \rho \mathbf{g}). \tag{2}$$

In equation (2) the permeability K is constant and the fluid viscosity μ is also a non-linear function of temperature T. In addition, the Fourier constitutive equation for heat conduction and Maxwell–Gibbs relations for the system internal energy can be used. Therefore, the energy balance results as follows:

$$c\nabla \cdot (\rho \mathbf{v} T) = \nabla \cdot (k_m \nabla T) - T\left(\frac{\partial p}{\partial T}\right)_\rho \nabla \cdot \mathbf{v}. \tag{3}$$

In equation (3) the heat capacity c is taken as constant, either for air or water, because its variation with T is negligible in a wide range of temperatures. Since the energy balance describes the system thought of as a mixture (fluid and solid matrix) we have defined the effective heat conduction through the following equation (see also, Gartling and Hickox [5]):

$$k_m(T) = \phi k(T) + (1 - \phi)k_s \tag{4}$$

ϕ being the porous medium porosity. Moreover, it is found that k_m varies with temperature only through the fluid conductivity $k(T)$, which is also a non-linear function of T, and that k_s is independent of temperature.

Equations (1)–(3) are next written in terms of the

dimensionless stream function ψ and temperature θ with the same scales and symbols used by Prasad and Kulacki [1], which are presented here in the Nomenclature. However, it should be observed that the stream function has to be redefined in this work as follows:

$$u = -\frac{\alpha}{D}\frac{\partial\psi}{\partial Y}\left(\frac{\rho_h}{\rho}\right) \tag{5}$$

$$v = \frac{\alpha L}{D^2}\frac{\partial\psi}{\partial X}\left(\frac{\rho_h}{\rho}\right) \tag{6}$$

so that mass balance (equation (1)) is satisfied when the Boussinesq approximation is eliminated. From equation (2) we can evaluate the term $\nabla\times(\mu\mathbf{v})$ which combined with equations (5) and (6) yields

$$A^2\frac{\partial}{\partial X}\left(\frac{M}{R}\frac{\partial\psi}{\partial X}\right)+\frac{\partial}{\partial Y}\left(\frac{M}{R}\frac{\partial\psi}{\partial Y}\right)=Ra^*\frac{A}{B}\frac{\partial R}{\partial X} \tag{7}$$

where $Ra^* = Kg\beta\Delta T\rho_h/\mu_h U$ is the Rayleigh number evaluated at T_h, $A = L/D$ is the aspect ratio and $B = \beta\Delta T$ is the dimensionless fluid coefficient of thermal expansion. In equation (7) we have also defined the dimensionless viscosity $M(\theta)$ and density $R(\theta)$ as functions of dimensionless temperature θ (see the Appendix).

Equation (3) can be combined with equations (5) and (6) in order to obtain the following dimensionless equation:

$$-\frac{\partial}{\partial X}\left(\theta\frac{\partial\psi}{\partial Y}\right)+\frac{\partial}{\partial Y}\left(\theta\frac{\partial\psi}{\partial X}\right)$$
$$=\frac{\partial}{\partial X}\left(F\frac{\partial\theta}{\partial X}\right)+\frac{1}{A^2}\frac{\partial}{\partial Y}\left(F\frac{\partial\theta}{\partial Y}\right)$$
$$-(\theta+\Lambda)\gamma\left[-\frac{\partial}{\partial X}\left(\frac{1}{R}\frac{\partial\psi}{\partial Y}\right)+\frac{\partial}{\partial Y}\left(\frac{1}{R}\frac{\partial\psi}{\partial X}\right)\right] \tag{8}$$

where $F(\theta)$ is the dimensionless effective conductivity as a function of dimensionless temperature (see the Appendix). Since $\theta = (T-T_c)/(T_h-T_c)$, a new parameter $\Lambda = T_c/(T_h-T_c)$ is necessary to introduce in the pressure work term. In equation (8), γ is defined as

$$\gamma = \frac{1}{\rho_h c}\left(\frac{\partial p}{\partial T}\right)_\rho = -\frac{1}{\rho_h c}\frac{(\partial\rho/\partial T)_p}{(\partial\rho/\partial p)_T}. \tag{9}$$

In the dimensionless analysis presented here the unknown characteristic velocity is $U = k_{mh}/(\rho_h cD)$, which is consistent with the analysis of Prasad and Kulacki [1].

Hydrodynamics and thermal boundary conditions are

$$\psi = 0, \quad \theta = 1 \quad \text{at} \quad X = 0 \tag{10}$$

$$\psi = 0, \quad \theta = 0 \quad \text{at} \quad X = 1 \tag{11}$$

$$\psi = 0, \quad \frac{\partial\theta}{\partial Y} = 0 \quad \text{at} \quad Y = 0 \text{ and } 1. \tag{12}$$

In order to explain physically these boundary conditions, one has to observe that the fluid does not leave the porous cavity, which implies that the normal component of fluid velocity at the walls is zero. Also, adiabatic walls require that heat conduction flux be zero, while vertical walls have a prescribed value of temperature.

Once the flow and temperature fields are numerically solved, we can evaluate two Nusselt numbers as follows:

$$Nu_h = \int_0^1 \left(\frac{\partial\theta}{\partial X}\right)_{X=0} dY \tag{13}$$

at the hot wall and

$$Nu_c = F(\theta=0)\int_0^1 \left(\frac{\partial\theta}{\partial X}\right)_{X=1} dY \tag{14}$$

at the cold wall.

Central finite difference equations are derived from the divergence form of equations (7) and (8); however, second upwind differences for the convective terms [6] are introduced in the energy balance. In order to solve the simultaneous algebraic equations that result from the discretization process, a point iterative method is applied which makes use of the new values at each grid point as soon as they are available. A convergence criterium is defined according to the following norms:

$$\frac{\sum_{ij}|\psi_{ij}^n-\psi_{ij}^{n-1}|}{\sum_{ij}|\psi_{ij}^n|}\leqslant\varepsilon$$

and

$$\frac{\sum_{ij}|\theta_{ij}^n-\theta_{ij}^{n-1}|}{\sum_{ij}|\theta_{ij}^n|}\leqslant\varepsilon$$

where ij imply spatial position in the computational mesh and n refers to the iteration number. ε was fixed at 10^{-5} because the numerical method yields almost the same Nusselt numbers as those obtained when $\varepsilon = 10^{-6}$ (differences do not exceed 1%) at a lower computational cost.

To accelerate convergence, the temperature field is initialized with the analytic solution of equation (8) in the particular case when $A = 0$. For low Rayleigh numbers, over-relaxation of the temperature matrix accelerates convergence, and for high Rayleigh numbers, under-relaxation is appropriate to compute the stream function. The over-relaxation parameter is varied between 1 and 1.9, whereas a suitable value for the under-relaxation parameter is between 0.5 and 0.9. Also, temperature gradients at the horizontal walls are evaluated using two-point formulas for the derivatives.

Table 1. Meshes used for different values of Ra^* and A

Ra^*	50	100	1000	2000	5000	10000
$A = 0.3$	31×21	31×21	41×31	41×31	41×31	41×31
$0.5 \leqslant A \leqslant 1$	31×31	31×31	41×41	41×41	41×41	41×41
$2 \leqslant A \leqslant 3$	21×31	21×31	31×41	31×41	31×41	31×41

In the present work, grid intervals ΔX and ΔY are continuously varied following the method proposed by Kálnay de Rivas [7]. Therefore, a new coordinate system (ξ, η) needs to be defined so that

$$X = \sin^2\left(\frac{\pi}{2}\xi\right) \tag{15}$$

$$Y = \sin^2\left(\frac{\pi}{2}\eta\right). \tag{16}$$

In the new coordinate system the grid intervals $\Delta\xi$ and $\Delta\eta$ have to be chosen as constant. With this coordinate system, very fine grid intervals for X and Y can be obtained near vertical walls, particularly when boundary layers are present for large Rayleigh numbers. Mesh sizes of the order of 0.0015 can be obtained near walls for $Ra^* \geqslant 1000$ and $A \leqslant 1$.

Table 1 shows meshes used for different Rayleigh numbers and aspect ratios. These mesh sizes allowed us to obtain an acceptable invariance of results when $\Delta\eta$ and $\Delta\xi$ are changed.

Consistency of numerical results can be verified from a physical point of view by performing a macroscopic energy balance in the porous cavity, i.e. the heat flux that enters the cavity through the hot wall has to be equal to the heat flux that leaves the cavity at the cold wall. Consequently, it is required that

$$Nu_h = Nu_c. \tag{17}$$

This energy balance was satisfied within 1% for 94% of the cases reported here, whereas the error was within 2% for the rest (see also Prasad and Kulacki [1]). Therefore, through this work we designate $Nu = Nu_h = Nu_c$, and Nu_B is the Nusselt number when the Boussinesq approximation is imposed.

We have also carried out numerical evaluations when equation (8) is discretized by using the first upwind differencing scheme (see, e.g. ref. [6]). Although the energy balance (equation (17)) is well satisfied, this method yields Nusselt numbers which are substantially different from those of the second upwind difference scheme. Therefore, the first upwind method is not recommended for this kind of problem and our conclusion is the same as that already reported by Prasad and Kulacki [1].

It is also important to mention here, that the classical central finite difference discretization procedure can only be used accurately at low Rayleigh numbers. To be more precise, we found that it can be used for $Ra^* < 1000$ when $A < 1$.

RESULTS AND DISCUSSION

When the Boussinesq approximation is imposed (i.e. $\gamma = 0$ and $F = 1$ in equation (8); $M = R = 1$ and $\partial R/\partial X = -B(\partial\theta/\partial X)$ in equation (7)), our results are in good agreement with those previously reported by Prasad and Kulacki [1, 4]. In fact, Table 2 shows that only small differences between Nusselt numbers Nu_B are found for large Rayleigh numbers and low geometric aspect ratios. These differences do not exceed 12%, and they are a consequence of the more refined grid used. Nevertheless, the Rayleigh number at which the flow structure changes from unicellular to multicellular convection does not agree with that reported by these authors when $A = 0.5$. Thus, our numerical evaluations establish that cellular change is produced for $Ra^* < 100$. This result was obtained with and without the coordinate transformation, with a different number of grid points (21×21, 31×31 and 41×41) in both the X- and Y-directions and with two- and three-point formulas for derivatives.

Throughout the present discussion, equations (7) and (8) are designated the complete model. Therefore, we performed calculations with this model for the following two cases: water (Case I) and air (Case II). The results obtained are next discussed and compared with their counterpart that arises when the Boussinesq approximation is imposed.

In order to evaluate the Rayleigh number, which is proportional to (ΔTD), we consider three different porous cavity widths, D: 200, 20 and 2 m, while ΔT is varied from 1 to 200°C.

Case I: water

Table 3 shows numerical values of Nusselt number Nu for different aspect ratios A and for $D = 200$ m. These results are of particular interest in geothermal reservoirs (see, e.g. ref. [8]).

If Table 3 is compared with Table 2 we find that Nu is greater than Nu_B for $Ra^* \leqslant 2000$ ($\Delta T \leqslant 40$°C); on the other hand, the opposite situation is true for $Ra^* > 2000$ ($\Delta T > 40$°C). Also, for $Ra^* \leqslant 2000$, differences between Nu and Nu_B do not exceed 10%, while for $Ra^* = 10000$ we find differences as large as 50%, independently of the value of A.

In order to explain that $Nu < Nu_B$ for $\Delta T > 40$°C, one has to observe that the relation between the Prandtl number evaluated at the local temperature θ and the Prandtl number referred to the hot temperature, $\theta = 1$, is approximately unity or slightly greater than one for $\Delta T \leqslant 40$°C, and it is greater than one for

Table 2. Selected values of Nu_B for various Ra^* and aspect ratios, from our numerical results and from the results of Prasad and Kulacki

		Ra^*	50	100	1000	2000	5000	10000
$A = 0.3$	This work	Nu_B	1.14	1.39	10.11	18.99	38.19	59.25
		Flow structure	u	m	m	m	m	m
	P & K	Nu_B	1.13	—	10.66	—	41.46	67.00
		Flow structure	u	m	m	m	m	m
$A = 0.5$	This work	Nu_B	1.45	2.19	13.62	22.03	38.47	55.89
		Flow structure	u	u	m	m	m	m
	P & K	Nu_B	1.43	—	14.21	—	43.68	62.58
		Flow structure	u	m	m	m	m	m
$A = 0.7$	This work	Nu_B	1.74	2.73	13.83	21.14	35.35	50.46
		Flow structure	u	m	m	m	m	u
	P & K	Nu_B	1.69	—	13.51	—	38.95	55.52
		Flow structure	u	m	m	m	m	u
$A = 0.9$	This work	Nu_B	1.93	3.00	13.29	19.79	32.47	46.03
		Flow structure	u	u	m	m	u	u
	P & K	Nu_B	1.96	—	14.19	—	35.49	50.20
		Flow structure	u	u	m	m	u	u
$A = 1$	This work	Nu_B	1.95	3.03	12.95	19.15	31.21	44.17
		Flow structure	u	u	m	u	u	u
	P	Nu_B	2.01	3.17	14.62	21.51	33.58	48.18
$A = 2$	This work	Nu_B	1.95	2.87	10.16	14.51	22.81	31.62
		Flow structure	u	u	u	u	u	m
	P	Nu_B	1.94	2.97	11.26	—	22.45	35.27
$A = 3$	This work	Nu_B	1.44	2.50	8.52	12.09	18.89	26.41
		Flow structure	u	u	u	u	u	m

u, unicellular flow.
m, multicellular flow.
P & K, results reported in ref. [1].
P, results reported in ref. [4].

$\Delta T > 40°C$. This relation can be evaluated directly from $M(\theta)/F(\theta)$ and when it is greater than one, the variable temperature fluid has less thermal conductivity and more viscosity than the Boussinesq fluid.

Although for $\Delta T < 40°C$, the relation $M(\theta)/F(\theta) \approx 1$, differences between Nu and Nu_B are due to the pressure work term in equation (8). Moreover, these differences present a minimum when $Ra^* \sim 2000$ ($\Delta T \sim 40°C$) for all values of A. In fact, at this point, the effects on the heat transfer associated with thermal changes in $M(\theta)/F(\theta)$ and in the pressure work term compensate each other.

From Table 3 it is concluded that the Nusselt number does not always increase for a fixed value of A. This is so because our complete model is able to evaluate the exponential water viscosity decrease with ΔT; therefore, when the temperature difference across the porous cavity is near 100°C, the viscosity variation becomes important on $M(\theta)/F(\theta)$ and the heat transfer decreases.

From Table 3 it is also interesting to analyse the effect of the aspect ratio on Nu. Thus, it is concluded that increasing A, the following trends are obtained:

(a) Nu decreases for $A \geqslant 1$ and $Ra^* > 0$;
(b) Nu increases for $A < 1$ and $Ra^* < 1000$;
(c) Nu decreases for $A < 1$ and $Ra^* > 7500$.

However, if $1000 \leqslant Ra^* \leqslant 7500$ and $A < 1$, the Nusselt number is not a monotonic function of A. This has also been observed by Prasad and Kulacki [1].

Figure 1 shows the relation Nu/Nu_B as a function of Ra^* for different porous cavity widths. When $D = 2$ m, Nu/Nu_B is less than one for all Rayleigh numbers; on the other hand, for $D = 20$ and 200 m there exists a range of Rayleigh numbers in which $Nu > Nu_B$. In Fig. 1, smaller ΔT are required to obtain a fixed value

Table 3. Selected values of Nu for various Ra^* and aspect ratios when $D = 200$ m (Case I)

Ra^*	50	100	1000	2000	5000	7500	8500	10000
ΔT	1	2	20	40	100	150	170	200
$A = 0.3$	1.2	1.47	11.05	18.82	29.43	31.11	30.65	29.42
$A = 0.5$	1.51	2.44	14.47	21.55	30.19	31.18	30.65	29.28
$A = 0.7$	1.89	3.07	14.53	20.60	27.93	28.66	28.12	26.84
$A = 0.9$	2.11	3.34	13.90	19.26	25.72	26.32	25.83	24.60
$A = 1$	2.17	3.40	13.51	18.64	24.75	25.30	24.84	23.67
$A = 2$	2.14	3.16	10.52	14.05	18.11	18.42	18.12	17.28
$A = 3$	1.90	2.75	8.82	11.72	15.10	15.38	15.14	14.43

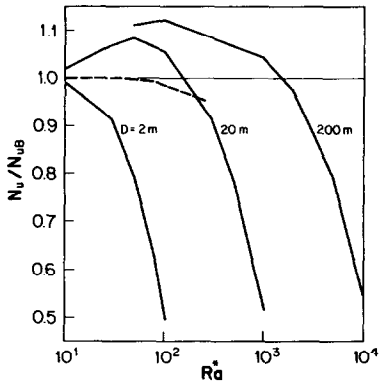

FIG. 1. Nu/Nu_B as a function of Ra^* when the fluid is water (Case I), $T_h = 200°C$. The dashed line refers to the results reported by Gartling and Hickox [5].

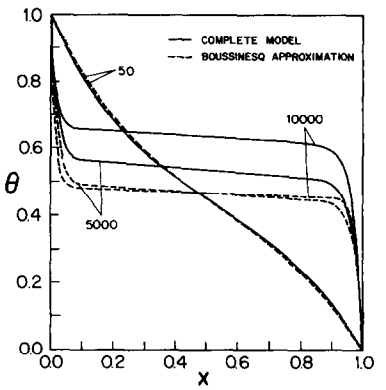

FIG. 2. Temperature distribution at the vertical midplane, $Y = 0.5$, for $A = 1$ and $D = 200$ m (Case I).

of Ra^* when D increases. Therefore, the effect of the pressure work is more important than the effect of the local Prandtl number, on the heat transfer.

It is also interesting to mention here that Blythe and Simpkins [9] studied thermal convection in a fluid saturated porous layer through integral relations, in the high Rayleigh number limit, for a temperature dependent fluid viscosity. Moreover, their calculations consider a linear relation between $\mu(\theta = 0)/\mu(\theta)$ and θ. When their results (see Fig. 7 and equation (4-10) of ref. [9]) are applied to the case in which water is the fluid that fills the porous cavity, it is inferred that Nu is slightly greater than Nu_B for $Ra^* \leqslant 10000$ ($\Delta T \leqslant 200°C$). Taking into account that Blythe and Simpkins [9] used the cold wall temperature as the reference temperature, we conclude here that the trend of their results is in good agreement with ours, although greater differences between Nu and Nu_B are expected in their work with a more realistic functionality between $\mu(\theta = 0)/\mu(\theta)$ and θ.

In order to compare our results with those reported by Gartling and Hickox [5], it should be observed that in their work a Rayleigh number equal to 300 implies a $\Delta T = 70°C$, hence the system studied by these authors yields values that lie between the curves corresponding to $D = 20$ and 2 m, and they are illustrated by a dashed line in Fig. 1.

Figure 2 shows the temperature profile at the midheight of the porous cavity when $A = 1$ and $D = 200$ m for different Ra^*, obtained from the numerical solution of the complete model (full lines) and when the Boussinesq approximation is considered (dashed lines). For $Ra^* = 50$ ($\Delta T = 1°C$) temperature profiles computed from both models are similar. However, for $Ra^* = 5000$ ($\Delta T = 100°C$) the curves of θ as a function of X depend substantially upon which model is used. Results illustrated in Fig. 2, show that large values of Ra^* are associated with sharp temperature drops near the vertical walls due to the boundary layer formation, as it is expected, while in the core region the temperature is linear in X for the complete model and it is almost constant when the Boussinesq approximation is considered. Also, in this last case, θ as a function of X and at $Y = 0.5$, is practically invariant for $Ra^* \geqslant 5000$.

If $Ra^* \geqslant 2000$ the slope $d\theta/dX$, near vertical walls, for the complete model is always smaller than the slope for the Boussinesq approximation; this is consistent with the result that $Nu/Nu_B < 1$ for $Ra^* \geqslant 2000$. Since the transition from pure conduction to boundary layer regimes is a consequence of competition between heat conduction and heat convection, it is inferred that this transition has to occur at higher Rayleigh numbers than those predicted by considering the Boussinesq approximation, when water is the fluid that fills the porous cavity.

Figure 3 shows temperature distributions at $X = 0.5$ for two values of Ra^* when $A = 1$ and $D = 200$ m, for the complete model (full lines) and for the Boussinesq model (dashed lines). In this figure, linear temperature profiles in Y, of variable extension, are observed. Nevertheless, for large values of Ra^*, results corresponding to the complete model show that these linear regions are not placed in the middle zone of the porous cavity, as it always occurs when the Boussinesq approximation is used.

From curves shown in Figs. 2 and 3, and from all the examples discussed in Case I, it is concluded that the dimensionless temperature at the porous cavity

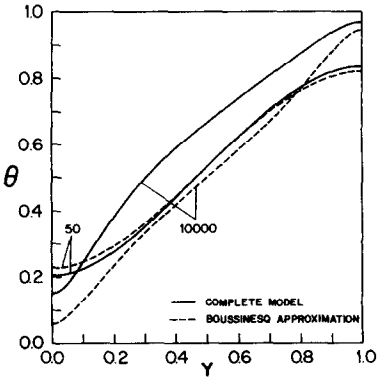

FIG. 3. Temperature distribution at the horizontal midplane, $X = 0.5$, for $A = 1$ and $D = 200$ m (Case I).

Table 4. Flow structure for various Ra^* and aspect ratios, for Boussinesq approximation (BA) and complete model (CM) in Case I ($D = 200$ m)

	Ra^*	50	100	1000	2000	5000	10 000
	ΔT	1	2	20	40	100	200
$A = 0.3$	CM	u	u	m	m	m	m
	BA	u	m	m	m	m	m
$A = 0.5$	CM	u	u	m	m	u	u
	BA	u	u	m	m	m	m
$A = 0.7$	CM	u	u	m	m	u	u
	BA	u	m	m	m	m	u
$A = 0.9$	CM	u	u	m	u	u	u
	BA	u	u	m	m	u	u
$A = 1$	CM	u	u	u	u	u	u
	BA	u	u	m	u	u	u
$A = 2$	CM	u	u	u	u	u	u
	BA	u	u	u	u	u	m
$A = 3$	CM	u	u	u	u	u	u
	BA	u	u	u	u	u	m

u, unicellular flow.
m, multicellular flow.

centre ($X = 0.5$ and $Y = 0.5$) is close to 0.5 only for $\Delta T < 40$°C when the complete model is considered. This result points out that the condition usually employed in approximate analysis, based upon the so-called 'centro symmetric property of the system' (see, e.g. ref. [10]) is only valid for low values of ΔT.

Numerical results obtained through the evaluation of the two models studied here, show important differences in flow structure as shown in Table 4, where multicellular flow (two recirculating cells) appears in a smaller range of Ra^*, when the fluid properties vary with temperature.

Figures 4 and 5 show the isotherms and streamlines for the complete model and the Boussinesq approximation when $Ra^* = 1000$ and $\Delta T = 200$°C. It is observed that isotherms are nearer the vertical walls in Fig. 5 (Boussinesq model) and that streamline distribution is remarkably affected by temperature-dependent fluid properties. The solution that belongs to the complete model (Fig. 4) does not show the centro symmetric property which is always observed in the Boussinesq solution (see Fig. 5 and results reported in ref. [1]). This asymmetry in the streamline distribution is a characteristic of the complete model solution and has been already reported by Gartling and Hickox [5] for small values of Ra^*. Our numerical evaluations show that when only one cell is present in the flow field and $\Delta T \geqslant 40$°C, the cell is displaced towards the hot wall of the porous cavity, if water is the fluid that fills the porous medium.

Case II: air

In this particular case the pressure of the system is maintained near 1 atm; hence air is assumed as an ideal gas. It is readily shown that equation (9) can be written as

$$\gamma = \frac{R(\theta)R_g}{M_w c}$$

where R_g is the gas-law constant and M_w is the average molecular weight of air.

It is clear that if air is the fluid that fills the porous cavity, the permeability of the porous medium must be considerably greater in order to obtain a Rayleigh number comparable to that of Case I, when the dimensions of the system are not changed (see the Appendix).

Table 5 shows Nusselt numbers obtained from the complete model when $D = 200$ m, for different aspect ratios A. From this table it is concluded that, increasing A, the following trends are obtained:

(a) Nu decreases for $A \geqslant 1$ and $Ra^* > 0$;
(b) Nu increases for $A < 1$ and $Ra^* < 1000$;
(c) Nu decreases for $A < 1$ and $Ra^* \geqslant 5000$.

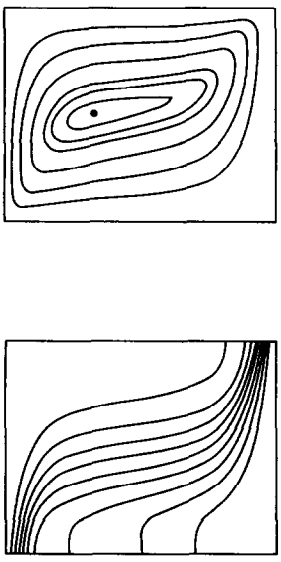

FIG. 4. Streamlines and isotherms for $Ra^* = 1000$ ($\Delta T = 200$°C) and $A = 1$ (Case I).

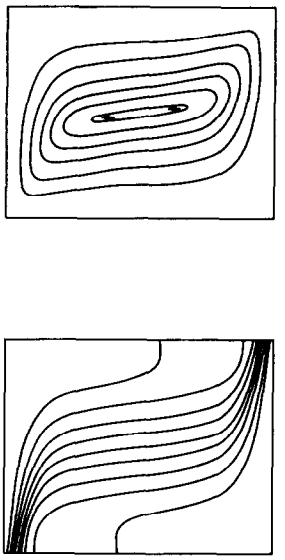

FIG. 5. Streamlines and isotherms for $Ra^* = 1000$ and $A = 1$ (Boussinesq approximation).

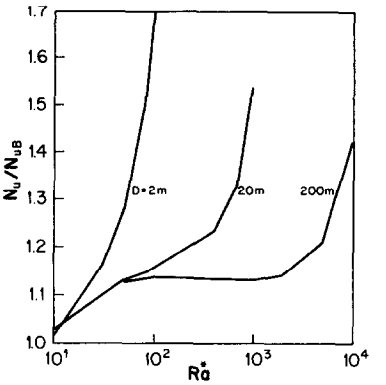

FIG. 6. Nu/Nu_B as a function of Ra^* when the fluid is air (Case II), $T_h = 200°C$.

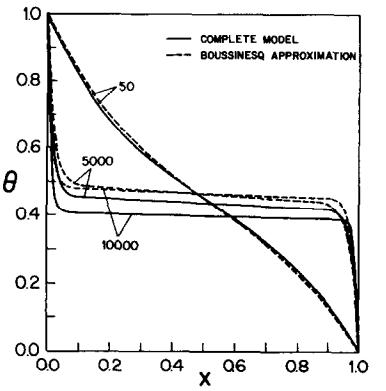

FIG. 7. Temperature distribution at the vertical midplane, $Y = 0.5$, for $A = 1$ and $D = 200$ m (Case II).

However, if $1000 \leqslant Ra^* < 5000$, the Nusselt number is not a monotonic function of A. A similar result has been observed in Case I and in ref. [1].

If Table 5 is compared with Table 2, it is concluded that $Nu/Nu_B > 1$. For a fixed value of A, differences between Nu and Nu_B are small ($\sim 5\%$) when $Ra^* = 50$ ($\Delta T = 1°C$) and increase for large Rayleigh numbers. Thus, the relative difference between Nu and Nu_B is around 36% when $Ra^* = 10\,000$ ($\Delta T = 200°C$). It is important to mention here that Zhong *et al.* [11] studied the effects of variable properties on temperature and velocity fields and heat transfer rate in a two-dimensional square enclosure filled with air. They conclude that the Boussinesq approximation predicts the overall heat transfer adequately, up to a value of $\Delta T = 50°C$. From our Tables 2 and 5, we find that differences between Nu and Nu_B do not exceed 13% for $\Delta T \leqslant 40°C$. Therefore, our results are in good agreement with those reported in ref. [11].

The trend followed by the relation Nu/Nu_B as a function of Ra^* in Case II, is different from that previously reported in Case I. In order to explain this result, one has to observe that air viscosity increases with temperature while the opposite is true for water viscosity; thus, in Case II the relation $M(\theta)/F(\theta)$ is less than one for all values of ΔT. Therefore, the effects on the heat transfer associated with thermal changes in $M(\theta)/F(\theta)$ and in the pressure work are additive.

Figure 6 shows Nu/Nu_B as a function of Ra^* for different porous cavity widths. As it is expected from our previous discussion, $Nu > Nu_B$ for all values of D and Ra^*.

Figure 7 shows the temperature profile at the midheight of the porous cavity when $A = 1$ and $D = 200$ m for different values of Ra^*, when the complete model (full lines) and the Boussinesq approximation (dashed lines) are considered. For $Ra^* = 50$ ($\Delta T = 1°C$) temperature profiles computed from both models are similar. However, for $Ra^* = 5000$ and 10 000, curves of θ as a function of X depend again substantially upon which model is used.

Table 5. Selected values of Nu for various Ra^* and aspect ratios when $D = 200$ m (Case II)

Ra^*	50	100	1000	2000	5000	10 000
ΔT	1	2	20	40	100	200
$A = 0.3$	1.20	1.49	12.46	23.36	49.39	88.96
$A = 0.5$	1.52	2.49	15.95	25.85	47.65	80.67
$A = 0.7$	1.91	3.13	15.89	24.44	43.32	72.47
$A = 0.9$	2.14	3.40	15.13	22.73	39.67	66.13
$A = 1$	2.20	3.45	14.72	21.96	38.11	63.50
$A = 2$	2.16	3.21	11.40	16.45	27.48	47.97
$A = 3$	1.92	2.79	9.54	13.71	22.94	40.02

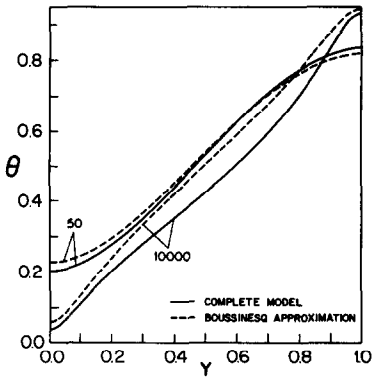

FIG. 8. Temperature distribution at the horizontal midplane, $X = 0.5$, for $A = 1$ and $D = 200$ m (Case II).

Also the slope $d\theta/dX$, near vertical walls, for the complete model is always greater than the slope for the Boussinesq model. Consequently, in this particular case the transition from pure conduction to boundary layer regimes occurs at lower Rayleigh numbers than those predicted with the Boussinesq approximation, which is a result different to that obtained in Case I.

Figure 8 shows the temperature distribution at $X = 0.5$ for two values of Ra^* when $A = 1$ and $D = 200$ m, obtained from the evaluation of the complete model (full lines) and the Boussinesq model (dashed lines). It is observed that curves θ–Y for air (Fig. 8) and water (Fig. 3) are similar when $Ra^* = 50$. However, for $Ra^* = 10\,000$, the functionality between θ and Y, at $X = 0.5$, depends substantially upon which fluid fills the porous cavity.

From the curves shown in Figs. 7 and 8 and from examples discussed in this case, the dimensionless temperature at the porous cavity centre ($A = 0.5$ and $Y = 0.5$) is only close to 0.5 for low values of ΔT when the complete model is evaluated. This result is the same as that reported for water in Case I.

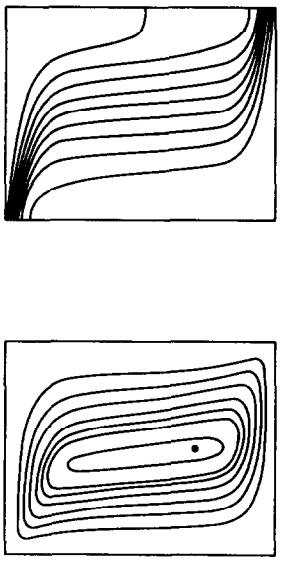

FIG. 9. Streamlines and isotherms for $Ra^* = 1000$ ($\Delta T = 200$°C) and $A = 1$ (Case II).

Numerical results obtained through the evaluation of both models show a different change in flow structure as shown in Table 6. These results and those presented in Table 4 point out that the criterion stated by Prasad and Kulacki [1] for the start of multicellular flow is no longer valid for the complete model, i.e. when fluid properties are dependent on temperature.

Figure 9 shows the isotherms and streamlines for the complete model when $Ra^* = 1000$ and $\Delta T = 200$°C. In this figure, the isotherms are nearer the vertical walls of the cavity than in Fig. 5 where the Boussinesq approximation is used. Also the streamline distribution is remarkably affected by temperature-dependent fluid properties, and the solution does not present the centro-symmetric property as in

Table 6. Flow structure for various Ra^* and aspect ratios, for Boussinesq approximation (BA) and complete model (CM) in Case II ($D = 200$ m)

	Ra^*	50	100	1000	2000	5000	10 000
	ΔT	1	2	20	40	100	200
$A = 0.3$	CM	m	m	m	m	m	m
	BA	u	m	m	m	m	m
$A = 0.5$	CM	u	u	m	m	m	u
	BA	u	u	m	m	m	m
$A = 0.7$	CM	u	u	m	m	u	u
	BA	u	m	m	m	m	u
$A = 0.9$	CM	u	u	m	m	u	u
	BA	u	u	m	m	u	u
$A = 1$	CM	u	u	u	u	u	u
	BA	u	u	m	u	u	u
$A = 2$	CM	u	u	u	u	m	m
	BA	u	u	u	u	u	m
$A = 3$	CM	u	u	u	u	m	m
	BA	u	u	u	u	u	m

u, unicellular flow.
m, multicellular flow.

Case I, which is always observed in the solution of the Boussinesq model. However, when one recirculating cell is present in the flow field at $\Delta T \geqslant 40°C$, this cell is displaced toward the hot wall in Case I, while in Case II it is displaced toward the cold wall of the cavity.

CONCLUSIONS

From our numerical study we conclude:

(1) If the temperature difference across the porous cavity is increased, i.e. increasing the Rayleigh number for a fixed value of aspect ratio, the Boussinesq solution shows a progressive departure from the solution of the complete model described in this work.

(2) If water is the fluid that fills the porous cavity (Case I), the relation Nu/Nu_B as a function of Ra^*, can be either lower or greater than one when the cavity width is sufficiently large. However, for small values of D, this relation is always less than one.

(3) If air is the fluid that fills the porous cavity (Case II), the relation Nu/Nu_B as a function of Ra^* is greater than one for all values of D.

(4) If water is the fluid that fills the porous cavity, the change from pure conduction to boundary layer flow regimes takes place at larger Rayleigh numbers than those predicted with the Boussinesq model. However, the opposite is true if the fluid is air.

(5) Asymmetries in flow fields are observed for $\Delta T \geqslant 40°C$. For the unicellular flow regime, the centre of the cell is displaced toward the hot wall for water and toward the cold wall for air.

Acknowledgements—The authors are grateful to the Consejo Nacional de Investigaciones Científicas y Técnicas (CONICET) and to the Universidad Nacional del Litoral (UNL) (Santa Fe, Argentina) for their support in producing this work.

REFERENCES

1. V. Prasad and F. A. Kulacki, Convective heat transfer in a rectangular porous cavity—effects of aspect ratio on flow structure and heat transfer, *ASME J. Heat Transfer* **106,** 158–165 (1984).
2. S. A. Bories and M. A. Combarnous, Natural convection in a sloping porous layer, *J. Fluid Mech.* **57,** 63–79 (1973).
3. K. L. Walker and G. M. Homsy, Convection in a porous cavity, *J. Fluid Mech.* **97,** 449–474 (1978).
4. V. Prasad, Natural convection in porous media. An experimental and numerical study for vertical annulus and rectangular enclosures, Ph.D. Thesis, University of Delaware, Newark (1983).
5. D. K. Gartling and C. E. Hickox, A numerical study of the applicability of the Boussinesq approximation for a fluid-saturated porous medium, *Int. J. Numer. Meth. Fluids* **5,** 995–1013 (1985).
6. P. J. Roache, *Computational Fluid Dynamics*, pp. 64–74. Hermosa, Albuquerque, New Mexico (1976).
7. E. Kálnay de Rivas, On the use of nonuniform grids in finite-difference equations, *J. Computational Phys.* **10,** 202–210 (1972).
8. P. Cheng, Heat transfer in geothermal systems, *Adv. Heat Transfer* **14,** 1–100 (1978).
9. P. A. Blythe and P. G. Simpkins, Convection in a porous layer for a temperature dependent viscosity, *Int. J. Heat Mass Transfer* **24,** 497–506 (1981).
10. A. Bejan and C. L. Tien, Natural convection in a horizontal porous medium subjected to an end-to-end temperature difference, *ASME J. Heat Transfer* **100,** 191–198 (1978).
11. Z. Y. Zhong, K. T. Yang and J. R. Lloyd, Variable property effects in laminar natural convection in a square enclosure, *ASME J. Heat Transfer* **107,** 133–138 (1985).
12. R. Perry, D. W. Green and J. Maloney, *Chemical Engineer's Handbook*, 6th Edn, Chap. 3. McGraw-Hill, New York (1984).

APPENDIX: POROUS MEDIUM AND FLUID PROPERTIES USED IN CASES I AND II

Case I: water

$$\rho_h = 0.8\,\mathrm{g\,cm^{-3}}$$
$$\beta = 2\times10^{-3}\,°\mathrm{C^{-1}}$$
$$c = 5.01\,\mathrm{J\,g^{-1}\,°C^{-1}}$$
$$\mu_h = 1.07\times10^{-3}\,\mathrm{g\,cm^{-1}\,s^{-1}}$$
$$k_{mh} = 1.94\times10^{-2}\,\mathrm{J\,cm^{-1}\,s^{-1}\,°C^{-1}}$$
$$K = 0.809\times10^{-8}\,\mathrm{cm^2}$$
$$\phi = 0.4$$

with these values the Rayleigh number can be written as

$$Ra^* = 2.5\times10^{-3}\,\Delta TD$$

where ΔT is in °C and D in cm.

From data reported in the literature [12] we find

$$R(\theta) = 1-0.002[\Delta T(\theta-1)]-0.4058\times10^{-5}[\Delta T(\theta-1)]^2 - 0.2455\times10^{-8}[\Delta T(\theta-1)]^3$$

$$M(\theta) = \frac{10^{248/[\Delta T(\theta+A)-140]}}{10^{248/[\Delta T(1+A)-140]}}$$

$$F(\theta) = \{2.59\phi[1+0.005345[\Delta T(\theta-1)] + 0.14\times10^{-4}[\Delta T(\theta-1)]^2 + 0.186\times10^{-7}[\Delta T(\theta-1)]^3] + 1.5(1-\phi)\}/[2.59\phi+1.5(1-\phi)].$$

Case II: air

$$\phi = 0.4$$
$$\rho_h = 0.743\times10^{-3}\,\mathrm{g\,cm^{-3}}$$
$$\beta = 2\times10^{-3}\,°\mathrm{C^{-1}}$$
$$c = 1.05\,\mathrm{J\,g^{-1}\,°C^{-1}}$$
$$\mu_h = 2\times10^{-4}\,\mathrm{g\,cm^{-1}\,s^{-1}}$$
$$k_{mh} = 0.91\times10^{-2}\,\mathrm{J\,cm^{-1}\,s^{-1}\,°C^{-1}}$$
$$K = 3.9\times10^{-3}\,\mathrm{cm^2}.$$

with these values the Rayleigh number can be written as

$$Ra^* = 2.5\times10^{-3}\,\Delta TD$$

where ΔT is in °C and D in cm.

From data reported in the literature [12] we find

$$R(\theta) = 1-0.002[\Delta T(\theta-1)]-0.168\times10^{-7}[\Delta T(\theta-1)]^3$$
$$M(\theta) = 1+0.001[\Delta T(\theta-1)]-0.124\times10^{-5}[\Delta T(\theta-1)]^2$$
$$F(\theta) = \{0.047\phi[1-0.00125[\Delta T(\theta-1)] - 0.73\times10^{-6}[\Delta T(\theta-1)]^2] + 1.5(1-\phi)\}/[0.047\phi+1.5(1-\phi)].$$

CONVECTION THERMIQUE NATURELLE DANS UNE CAVITE RECTANGULAIRE AVEC PROPRIETES VARIABLES DU FLUIDE—VALIDITE DE L'APPROXIMATION DE BOUSSINESQ

Résumé—L'applicabilité de l'approximation de Boussinesq est étudiée pour la convection naturelle dans une cavité poreuse saturée de fluide, avec des parois verticales maintenues à deux températures différentes, et des parois horizontales parfaitement isolées. Des calculs numériques sont conduits pour deux fluides d'intérêt pratique, l'eau et l'air, dans un large domaine de nombre de Rayleigh et de rapport de forme. On présente les champs de vitesse et de température, ainsi que les flux thermiques transférés, obtenus à partir d'un modèle avec la température. Une conclusion la plus importante est que le nombre de Nusselt évalué avec l'approximation de Boussinesq peut être sensiblement différent de celui obtenu avec ce modèle.

WÄRMETRANSPORT DURCH NATÜRLICHE KONVEKTION IN EINEM RECHTECKIGEN PORÖSEN KÖRPER MIT VARIABLEN FLUIDSTOFFWERTEN—GÜLTIGKEIT DER BOUSSINESQ-APPROXIMATION

Zusammenfassung—In dieser Arbeit wird die Brauchbarkeit der Boussinesq-Approximation für natürliche Konvektion in einem fluid-gesättigten, porösen Körper untersucht, dessen vertikale Wände auf zwei verschiedenen Temperaturen gehalten werden, und dessen horizontale Wände vollkommen isoliert sind. Es werden für zwei in der Praxis interessante Fluide, Wasser und Luft, numerische Berechnungen in einem weiten Bereich der Rayleigh-Zahl und des Seitenverhältnisses durchgeführt. Es werden Strömungs- und Temperaturfelder sowie Wärmeübergangskoeffizienten präsentiert, welche mit einem Modell berechnet wurden, das temperaturabhängige Stoffwerte für das Fluid berücksichtigt. Eine der wichtigsten Erkenntnisse ist, daß die über die Boussinesq-Approximation berechnete Nusselt-Zahl stark von der Nusselt-Zahl abweicht, die mit dem hier vorgestellten Modell berechnet wurde.

СВОБОДНОКОНВЕКТИВНЫЙ ТЕПЛООБМЕН ЖИДКОСТИ С ПЕРЕМЕННЫМИ СВОЙСТВАМИ В ПРЯМОУГОЛЬНОЙ ПОРИСТОЙ ПОЛОСТИ (ПРАВОМЕРНОСТЬ ПРИБЛИЖЕНИЯ БУССИНЕСКА)

Аннотация—Изучена возможность применения приближения Буссинеска в случае свободной конвекции в пористой насыщенной жидкостью полости, вертикальные стенки которой имеют разную температуру, а горизонтальные полностью теплоизолированы. Выполнены численные расчеты для двух различных сред (воды и воздуха) в широком диапазоне значений числа Рэлея и отношения длин сторон полости. Приведены результаты расчета полей температуры и скорости течения, а также интенсивностей теплообмена по модели, учитывающей зависимость свойств среды от температуры. Один из самых важных выводов заключается в том, что значения числа Нуссельта, полученные с помощью приближения Буссинеска и на основе принятой модели, могут существенно различаться.